IEEJ Journal of Industry Applications
Vol.7 No.6 pp.454–461 DOI: 10.1541/ieejjia.7.454

Paper

Simple and Effective Time Delay Compensation Method for Active Damping Control of Grid-Connected Inverter with an LCL Filter

Masaki Semasa* Non-member, Toshiji Kato* Fellow
Kaoru Inoue* Member

(Manuscript received Sep. 22, 2017, revised March 20, 2018)

A grid-connected inverter is equipped with an LCL filter at its output. This filter has a resonant characteristic and many active damping methods have been researched to suppress the resonant effects. The inverter is often controlled digitally and there is a control time delay, which is inevitable due to A/D conversion, computation times, etc. This delay degrades the stabilities and damping effects of the inverter because the frequency characteristics are different from the designed one, especially around the resonant frequency. This paper proposes a simple and effective compensation method of the control time delay to improve the damping effects. It is based on an estimation method of future state values advanced by the delay time. The proposed method is applied to the grid-connected inverter control and its effectiveness is investigated and validated through determining transfer functions of the regulated current errors by experiment.

Keywords: Grid-Connected inverter, control time delay compensation, active damping, digital control, z-transform, sinusoidal compensator

1. Introduction

A grid-connected inverter is equipped with an LCL filter at its output [(1)–(3)]. This filter has a resonant characteristic and many active damping methods have been researched to suppress the resonant effects [(4)–(17)]. However, the inverter is often controlled digitally and there is a control time delay, which is inevitable due to A/D conversion, computation times, etc. Effects of the delay have been extensively analyzed [(18)–(24)]. This delay degrades the inverter performances and frequency characteristics which are different from the designed ones. Especially the frequency characteristics around the resonant frequency of the filter are affected and they have large peaks and phase-shifts, which degrade the stability and damping effects. It is one of the most important subjects how to compensate the delay and realize the designed characteristics. Papers have been proposed and their principles are based on, for example, adjustment of the inverter output pulse width [(25)], modification of sampling methods [(26)(27)], duty ratio compensation [(28)], phase compensation [(29)], and so-called predictive control [(30)(31)].

This paper proposes a simple and effective compensation method of the control time delay to improve the damping effects. It is based on a new predictive estimation method which considers non-averaged modes of transients of the state variables during the delay time. After description of the proposed method, it is applied to a simple active damping control of a grid-connected inverter of a single-phase type with an LCL filter. Its effectiveness of the proposed compensation is investigated and validated through determining transfer functions of the regulated current errors experimentally by a DSP-based digital control system.

* Department of Electrical Engineering, Doshisha University
Kyotanabe, Kyoto 610-0321, Japan

2. Active Damping Control of Grid-Connected LCL-Type Inverter without Considering Control Time Delay

2.1 Discrete State Equations of Grid-Connected Inverter with an LCL Filter A digital control scheme is used for a grid PWM voltage-source inverter which is a single-phase full-bridge configuration and connected to a utility source of voltage v_s as in Fig. 1. An LCL filter of L_1, C, L_2 is inserted at the inverter output to convert the voltage input $v_i = Eu$ to the current output i_{L2} and to reduce its harmonic components sufficiently. The state variables of L_1, C, L_2 are denoted as i_{L_1}, v_C, i_{L_2} and their vector form sampled at $t = iT$ is as $\boldsymbol{x}[i]$ where T is a sampling time interval. Its input voltage $v_i[i]$ is generated according to its input $u[i]$ where E is DC voltage of the inverter source. Continuous and discrete state equations for the output current of L_2, $y[i] = i_{L2}[i]$, are as follows.

$$\dot{\boldsymbol{x}}(t) = \boldsymbol{A}_c\boldsymbol{x}(t) + \boldsymbol{b}_c u(t) + \boldsymbol{h}_c v_s(t), \quad y(t) = \boldsymbol{c}_c\boldsymbol{x}(t) \quad \cdots\cdots (1)$$

$$\boldsymbol{x}[i+1] = \boldsymbol{A}\boldsymbol{x}[i] + \boldsymbol{b}u[i] + \boldsymbol{h}v_s[i], \quad y[i] = \boldsymbol{c}\boldsymbol{x}[i] \quad \cdots\cdots (2)$$

where

$$\boldsymbol{A} = e^{\boldsymbol{A}_c T}, \quad \boldsymbol{b} = \int_0^T e^{\boldsymbol{A}_c\tau} d\tau \boldsymbol{b}_c,$$
$$\boldsymbol{c} = \boldsymbol{c}_c, \qquad \boldsymbol{h} = \int_0^T e^{\boldsymbol{A}_c\tau} d\tau \boldsymbol{h}_c \quad \cdots\cdots (3)$$

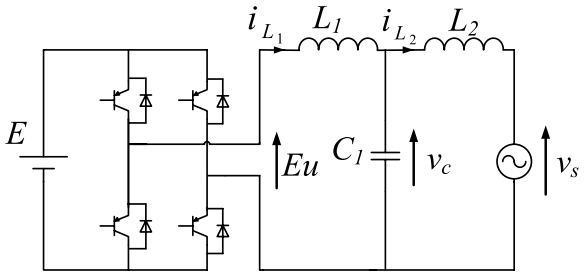

Fig. 1. Main circuit of a grid-connected inverter

$$\left.\begin{aligned}
\boldsymbol{A}_c &= \begin{bmatrix} 0 & 1/L_1 & 0 \\ 1/C & 0 & -1/C \\ 0 & 1/L_2 & 0 \end{bmatrix} \\
\boldsymbol{b}_c &= \begin{bmatrix} E/L_1 \\ 0 \\ 0 \end{bmatrix},\ \boldsymbol{h}_c = \begin{bmatrix} 0 \\ 0 \\ -1/L_2 \end{bmatrix} \\
\boldsymbol{x}(t) &= \begin{bmatrix} i_{L1}(t) \\ v_c(t) \\ i_{L2}(t) \end{bmatrix},\ \boldsymbol{c}_c = \begin{bmatrix} 0 & 0 & 1 \end{bmatrix}
\end{aligned}\right\} \cdots\cdots\cdots\cdots\cdots (4)$$

2.2 Digital Control System with a Time Delay

A digital control system is designed where the sinusoidal compensator is adopted to make the output y follow a reference y_{ref} [32]. The inverter is controlled according to a block diagram in Fig. 2(a) where f is frequency, s and z^{-1} are differential and one-sample delay operators, and $s = j2\pi f$ and $z = e^{-sT}$. All delays in blocks are unified into one delay block z^{-m} where the total delay time is $d = mT$ [μsec] ($0 < m$) from the i-th sampling to $u[i]$ output. The symbol $S_m(s) = (1 - e^{-sT})/(sT)$ stands for a frequency characteristic of the digital sampling. The sinusoidal compensator is used to eliminate steady-state errors for a reference sinusoidal waveform of an angular frequency ω_0. The transfer function of the compensator is as follows because its denominator is identical to that of z-transform of a sinusoidal waveform according to the internal model principle.

$$G[z] = \frac{k_2 z + k_1}{z^2 - 2\cos(\omega_0 T)z + 1} \cdots\cdots\cdots\cdots\cdots (5)$$

Two control gains k_1, k_2 in the numerator are design parameters.

The inverter input $u[i]$ is computed according to the following state feedback rule (6) where $w[i]$ and $w[i+1]$ are two auxiliary variables.

$$\left.\begin{aligned}
u[i] &= -\boldsymbol{f}\boldsymbol{x}[i] + k_1 w[i] + k_2 w[i+1] \\
w[i+2] &= -w[i] + 2\cos\omega_0 T w[i+1] \\
&\quad +(y_{ref}[i] - y[i])
\end{aligned}\right\} \cdots\cdots (6)$$

The final form of the proposed control scheme is as follows.

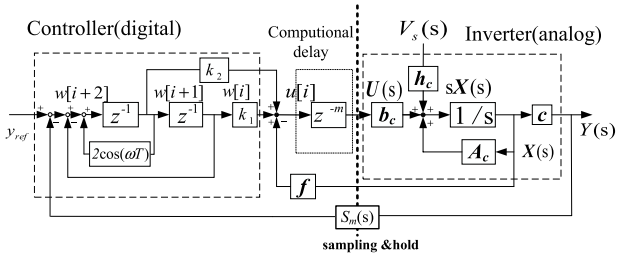

(a) Without control delay compensation

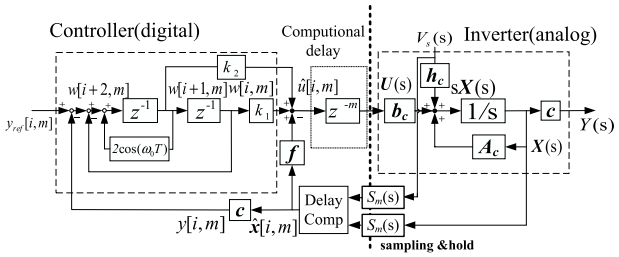

(b) With the proposed delay compensation

Fig. 2. Control block diagrams

$$\left.\begin{aligned}
\begin{bmatrix} \boldsymbol{x}[i+1] \\ w[i+1] \\ w[i+2] \end{bmatrix} &= \begin{bmatrix} \boldsymbol{A} & \boldsymbol{0} & \boldsymbol{0} \\ \boldsymbol{0} & 0 & 1 \\ -\boldsymbol{c} & -1 & 2\cos\omega T \end{bmatrix} \begin{bmatrix} \boldsymbol{x}[i] \\ w[i] \\ w[i+1] \end{bmatrix} \\
&+ \begin{bmatrix} \boldsymbol{b} \\ 0 \\ 0 \end{bmatrix} \begin{bmatrix} -\boldsymbol{f} & k_1 & k_2 \end{bmatrix} \begin{bmatrix} \boldsymbol{x}[i] \\ w[i] \\ w[i+1] \end{bmatrix} \\
&+ \begin{bmatrix} \boldsymbol{0} \\ 0 \\ 1 \end{bmatrix} y_{ref}[i] + \begin{bmatrix} \boldsymbol{h} \\ 0 \\ 0 \end{bmatrix} v_s[i] \\
&= \begin{bmatrix} \boldsymbol{A} - \boldsymbol{b}\boldsymbol{f} & \boldsymbol{b}k_1 & \boldsymbol{b}k_2 \\ \boldsymbol{0} & 0 & 1 \\ -\boldsymbol{c} & -1 & 2\cos\omega T \end{bmatrix} \begin{bmatrix} \boldsymbol{x}[i] \\ w[i] \\ w[i+1] \end{bmatrix} \\
&+ \begin{bmatrix} \boldsymbol{0} \\ 0 \\ 1 \end{bmatrix} y_{ref}[i] + \begin{bmatrix} \boldsymbol{h} \\ 0 \\ 0 \end{bmatrix} v_s[i]
\end{aligned}\right\} \cdots\cdots\cdots\cdots (7)$$

$$\hat{\boldsymbol{x}}[i+1] = \hat{\boldsymbol{A}}\hat{\boldsymbol{x}}[i] + \hat{\boldsymbol{h}} y_{ref}[i] + \hat{\boldsymbol{h}} v_s[i] \cdots\cdots\cdots\cdots (8)$$

Based on the above augumented system matrix $\hat{\boldsymbol{A}}$ and the input vector $\hat{\boldsymbol{h}}$, three feedback gains $\boldsymbol{f}$ and two compensator gains k_1, k_2 are determined according to the optimal control.

2.3 Active Damping Control with Virtual Resistors

A simple active damping control method with one virtual resistor is utilized to suppress the filter resonance oscillations. Inserting a resistor virtually just before the filter as in Fig. 3, it is possible to enhance the suppression effects. The inverter output voltage v_i is converted to v_i^* by the active damping control.

$$v_i^* = v_i - R_1 i_{L_1} \cdots\cdots\cdots\cdots\cdots\cdots\cdots\cdots\cdots (9)$$

This addition is effective to suppress the resonant peak of the filter characteristic. The resistor R_1 is adjusted to get enough attenuation of the resonant peak. The state feedback gains, $\boldsymbol{f}$, and the compensator gains, k_1, k_2, can be computed, for example, generally by the optimal control. The final feedback gain f_1^* of i_{L_1} becomes $f_1^* = f_1 + R_1/E$. Physical meaning of this resistor is that the inverter output power from the dashed rectangular is reduced by the consumption power of

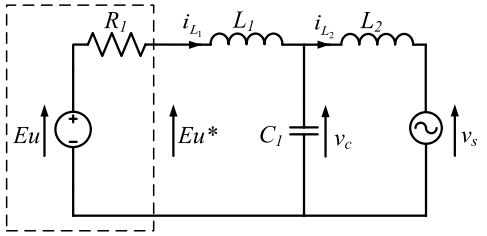

Fig. 3. Simple active control with a virtual resistor R_1

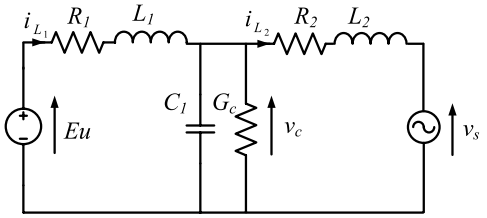

Fig. 4. Extended active control with virtual resistors R_1, R_2, G_c

Table 1. Inverter circuit parameters

parameters	value
input DC voltage	200 V
output voltage (rms)	100 V
output frequency	50 Hz
filter inductance L_1	0.76 mH
filter inductance L_2	0.76 mH
filter capacitance C	9.3 μF
switching and sample frequency	10 kHz

Table 2. Control gains

(a) With one virtual resistor

	optimal control
f	[0.0576, 0.0006, 0.0380]
k_1, k_2	-0.0241, 0.0289

(b) With three virtual resistors

	optimal control
f	[0.0566, 0.0022, 0.0360]
k_1, k_2	-0.0241, 0.0289

the resistor to damping oscillations.

This virtual damping method can be extended to a more general case which can consider a series resistor for a inductor and a parallel conductor for a resistor of any type of filters. For example, the circuit with the active damping control can be designed to behave similarly as the damping circuit in Fig. 4 with three resistors R_1, R_2, G_C. The idea is very simple that all eigenvalues for the two circuits after feedback controls are designed to have identical poles so that their damping effects behave similarly. The gain design is described in Appendix 1.

2.4 Simulated and Experimental Results with the Control Time Delay The simple active damping method is applied to the single-phase grid-connected inverter to investigate basic characteristics of TFs of the regulated current errors for the damping control, first, by simulation. The input DC voltage is 200 V, the system voltage 100 V(rms), $L_1 = L_2 = 0.76$ mH, and $C = 9.3\,\mu$F as listed in Table 1, and control gains are listed in Table 2(a). Simulated TF characteristics dependent on the delay time and they are shown

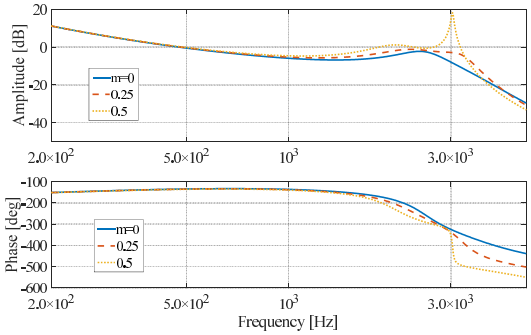

(a) Simulated time delay effects for $m = 0, 0.25, 0.5$ with $R_1 = 5\Omega$

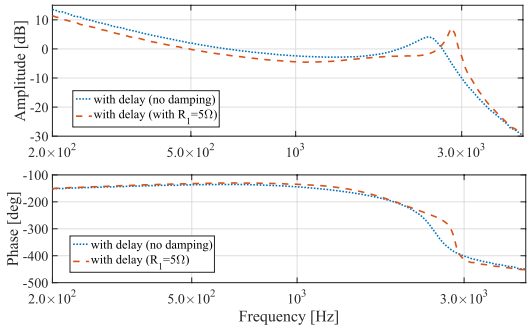

(b) Measured characteristics

Fig. 5. Frequency characteristics of transfer function of the regulated current errors

in Fig. 5(a) for $m = 0, 0.25, 0.5$ cases with $R_1 = 5\,\Omega$ and an assumed internal resistance $3\,\Omega$. Ideally the amplitude characteristic is almost flat. However, as m increases, the characteristic has a larger peak and the phase varies wider even for such a small m.

These undesirable effects are investigated experimentally. It is controlled with a DSP-based digital control system which has a time delay of 50 μsec at 100 μsec sampling time. The measured frequency characteristics of the TFs are shown in Fig. 5(b). The dotted blue curve shows the TF without the damping control and it has a peak around the resonant frequency of 2.7 kHz. The orange dashed curve shows the TF with the damping control and still it has a peak around the resonant frequency. Theoretically the characteristic should be damped. However, it is different from its designed characteristic because the control time delay affects the TF especially around the frequency. The time delay has to be compensated to damp the peak effectively.

3. Time Delay Compensation Method

3.1 Basic Idea based on Averaging As a time delay compensation method, this paper proposes to compute the control input u not at $t = iT$ but at $t = (i + m)T$ which is the advanced time by mT from $t = iT$. A future value $\hat{\boldsymbol{x}}[i, m]$ at $t = (i + m)T$ is estimated from $\boldsymbol{x}[i]$ at $t = iT$ and it is used to compute input $\hat{u}[i, m]$ using the modified z-transform as follows where $\boldsymbol{A_m}$, $\boldsymbol{b_m}$, $\boldsymbol{h_m}$ are coefficients of discrete state equations from $t = iT$ to $t = (i + m)T$.

$$\left.\begin{aligned}\hat{\boldsymbol{x}}[i, m] &= \boldsymbol{A}_m\boldsymbol{x}[i] + \boldsymbol{b}_m\hat{u}_d[i-1] + \boldsymbol{h}_m v_s[i] \\ \hat{u}[i, m] &= -\boldsymbol{f}\hat{\boldsymbol{x}}[i, m] + k_1 w[i, m] + k_2 w[i+1, m]\end{aligned}\right\} \quad \cdots\cdots\cdots\cdots\cdots (10)$$

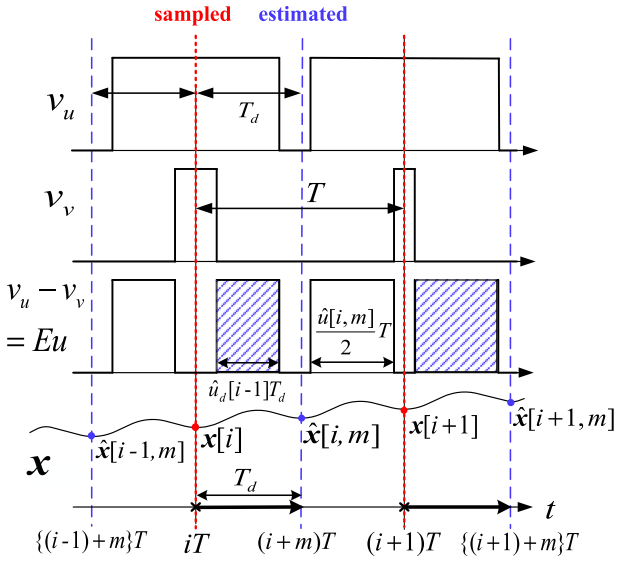

(a) Proposed compensation principle

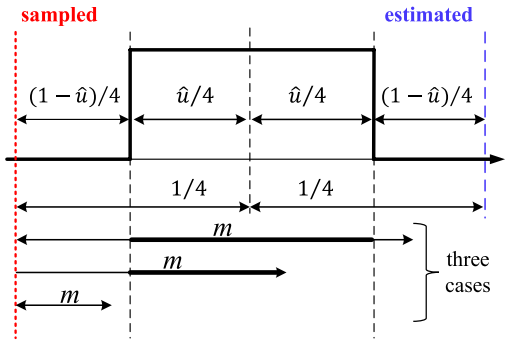

(b) Three cases for computation of the duty $\hat{u}_d[i-1]$ where $\hat{u} = \hat{u}[i-1,m]$

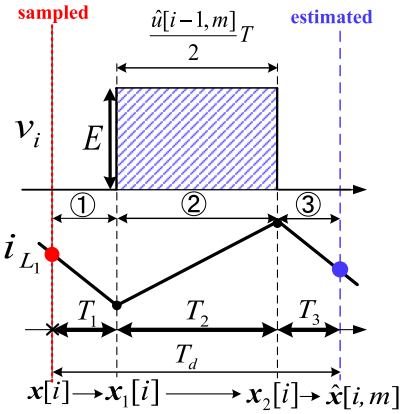

(c) Precise estimation of the inductor current i_{L_1}, considering three modes

Fig. 6. Proposed compensation principle

$$\boldsymbol{A}_m = e^{\boldsymbol{A}_c mT}, \quad \boldsymbol{b}_m = \int_0^{mT} e^{\boldsymbol{A}_c \tau} d\tau \boldsymbol{b}_c,$$
$$\boldsymbol{h}_m = \int_0^{mT} e^{\boldsymbol{A}_c \tau} d\tau \boldsymbol{h}_c \cdots\cdots\cdots (11)$$

This compensation principle is illustrated as in Fig. 6(a). State values are sampled as $\boldsymbol{x}[i-1], \boldsymbol{x}[i], \boldsymbol{x}[i+1], \cdots$. There is a time delay mT for generation of the inverter output pulse based on $u[i]$. The input $\hat{u}[i,m]$ at $t = (i+m)T$ is computed from $\hat{\boldsymbol{x}}[i,m]$ estimated by (10). An inverter pulse is output from $t = (i+m)T$ to $(i+1+m)T$ and it can be synchronized with $\hat{\boldsymbol{x}}[i,m]$.

A control block diagram with the proposed delay compensation is shown in Fig. 2(b). Based on the sampled values at $t = iT$, z^m-advanced state values at $t = (i+m)T$ are estimated, and they are used to compute $\hat{u}[i,m]$ which is an inverter input at $t = (i+m)T$ in the digital controller area. The input $\hat{u}[i,m]$ is ready at $t = iT$. However, there is the time delay z^{-m}, and the $\hat{u}[i,m]$ is actually delivered to the inverter at $t = (i+m)T$. The control delay z^{-m} is equivalently compensated by the *Delay Comp* block according to the above process.

It is noted that the inverter output length $\hat{u}_d$ which is shaded with blue dashes, must be precisely computed, considering timing relations. For example, when the delay time ratio is $m = 0.5$ as in Fig. 6(a), the dashed pulse $v_u - v_v$ which is one of the dual output pulses from $t = \{i + 0.25(1-|\hat{u}|)\}T$ to $t = \{i + 0.25(1+|\hat{u}|)\}T$ is completely covered during the delay time where $\hat{u}[i-1,m]$ is abbreviated simply as $\hat{u}$. When m varies between $0 \le m \le 0.5$, there are three cases for covering the pulse during the delay as in Fig. 6(b). The averaged duty ratio $\hat{u}_d[i-1]$ is expressed as follows.

$$|\hat{u}_d[i-1]| = \begin{cases} 0.5|\hat{u}|/m \\ \quad \text{if } 0.25(1+|\hat{u}|) < m < 0.5 \\ \{m + 0.25(|\hat{u}|-1)\}/m \\ \quad \text{if } 0.25(1-|\hat{u}|) < m < 0.25(1+|\hat{u}|) \\ 0 \\ \quad \text{if } m < 0.25(1-|\hat{u}|) \end{cases}$$
$$\cdots\cdots\cdots\cdots\cdots (12)$$

The term m in the denoninator expresses averaging operation during mT. The sign of $\hat{u}_d[i-1]$, or the polarity of the pulse, is directly dependent on that of $\hat{u}$.

$$\hat{u}_d[i-1] = \text{sign}(\hat{u})|\hat{u}_d[i-1]| \cdots\cdots\cdots\cdots\cdots\cdots (13)$$

Generally, the expression of $\hat{u}_d[i-1]$ is dependent on the delay ratio m because the covered pulse length is dependent on m.

3.2 State Estimation Considering Waveform Ripples

Utilizing the averaging method, the state variables can be estimated approximately. However, they are not precise because the inductor current i_{L_1} has large ripples. The state variables have to be estimated precisely from state equations without averaging.

The objective control system has a time delay of 0.5 sample, or $T_d = 0.5T$. As shown in Fig. 6(c), the time interval T_d from $t = iT$ to $t = (i+m)T$ is divided into three transition modes, (T_1, T_2, T_3) where T_2 is the shaded output pulse width $|\hat{u}[i-1,m]|T/2$ and the rest $mT - T_2$ is divided equally into T_1 and T_3 The current decreases, increases, and decreases, assuming the inverter output is a positive pulse. The situation is quite opposite when the inverter output is negative.

The state variables are precisely estimated from the following three equations which express state transients of the modes respectively. The sampling time assumed to be small enough and $v_s[i]$ can be approximated to be constant for the interval.

$$
\left.\begin{array}{ll}
① & \boldsymbol{x}_1[i] = \boldsymbol{A}_1\boldsymbol{x}[i] + \boldsymbol{h}_1 v_s[i] \\
 & \quad \text{for} \quad T_1 = 0.25(1 - |\hat{u}[i-1,m]|)T \\
② & \boldsymbol{x}_2[i] = \boldsymbol{A}_2\boldsymbol{x}_1[i] + \boldsymbol{b}_2 \text{sign}(u[i-1,m]) + \boldsymbol{h}_2 v_s[i] \\
 & \quad \text{for} \quad T_2 = 0.5|\hat{u}[i-1,m]|T \\
③ & \hat{\boldsymbol{x}}[i,m] = \boldsymbol{A}_3\hat{\boldsymbol{x}}_2[i] + \boldsymbol{h}_3 v_s[i] \\
 & \quad \text{for} \quad T_3 = T_1
\end{array}\right\} \cdots\cdots\cdots\cdots\cdots\cdots (14)
$$

where

$$
\boldsymbol{A}_n = e^{\boldsymbol{A}_c T_n}, \quad \boldsymbol{b}_n = \int_0^{T_n} e^{\boldsymbol{A}_c \tau} d\tau \boldsymbol{b}_c,
$$

$$
\boldsymbol{h}_n = \int_0^{T_n} e^{\boldsymbol{A}_c \tau} d\tau \boldsymbol{h}_c \qquad (n = 1, 2, 3) \cdots\cdots\cdots\cdots (15)
$$

These state modes are dependent on the delay time and the input duty. They have to be modified when they form a different combination of transition modes.

For example, the proposed method can be applied for a three-phase inverter of $m = 1$ case. The basic idea is the same that it is based on the proposed predictive estimation method which considers non-averaged modes of transients of the state variables during the delay time. In the three-phase case, the computation process of the inverter output voltage becomes more complex because it needs further consideration of modes of the neutral point voltage waveform [33].

4. Experimental Results of the Proposed Control with Compensation of the Time Delay

4.1 Effects of Control Delay Compensation and Active Damping with One Resistor First, the proposed compensation method is investigated to check the effectiveness. The purple pulse shows the scaled inverter output voltage Eu. The estimated current value $\hat{i}_{L1}[i,m]$ is checked if it is close enough to the actual value $i_{L1}[i,m]$ and the results are shown in Fig. 7(a). The oscillatory blue waveform is the current $i_{L1}(t)$ with ripples, its sampled values $i_{L1}[i]$ are denoted as the red curve, and the estimated values $\hat{i}_{L1}[i,m]$ are denoted as the yellow curve. The delay is half of the sampling time and the yellow actual values of $i_{L1}[i,m]$ are located almost in the center of the ripples. A zoomed figure is shown in Fig. 7(b). The yellow estimated $\hat{i}_{L1}[i,m]$ crosses the blue actual $i_{L1}(t)$ waveform at the estimated time $t = (i+m)T$.

Effects of the proposed damping control with one virtual resistor are investigated. The measured frequency characteristics of the TFs are shown and compared in Fig. 8(a). Without the delay compensation and the damping, the TF is shown as the blue dotted curve and it has a large resonant peak. After the compensation, the TF is shown with the yellow rigid curve and the peak is a little mitigated. After the damping with one virtual resistor, the TF is shown as the dashed red curve and the peak is considerably suppressed. However, the TF gain after the damping is a little reduced, and there is a trade-off between damping effects and control responses.

Not only the frequency characteristics but also time-domain waveforms are also investigated. The current waveform in Fig. 9(a) before the compensation has oscillations near zero-cross timings where control performances are affected apparently due to dead-time effects. Such oscillations are effectively suppressed as shown in Fig. 9(b) after the delay compensation and (c) after the damping with one-resistor.

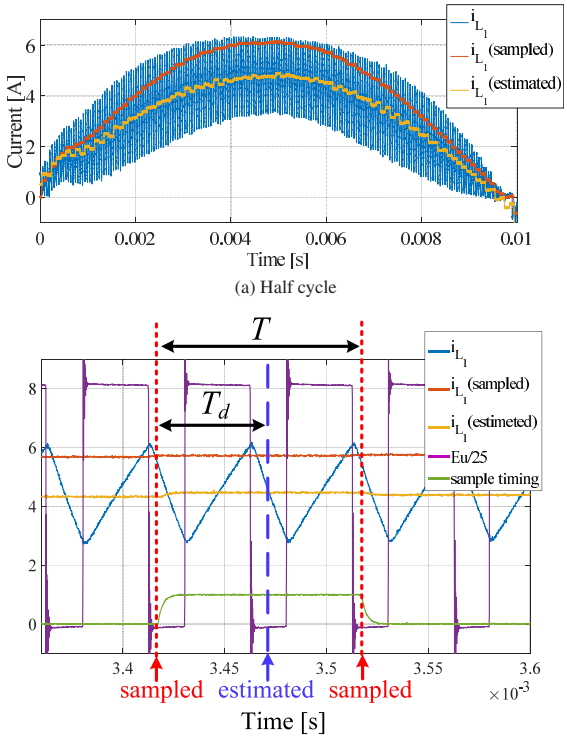

(a) Half cycle

(b) Zoomed

Fig. 7. Sampled and estimated current i_{L1} waveforms

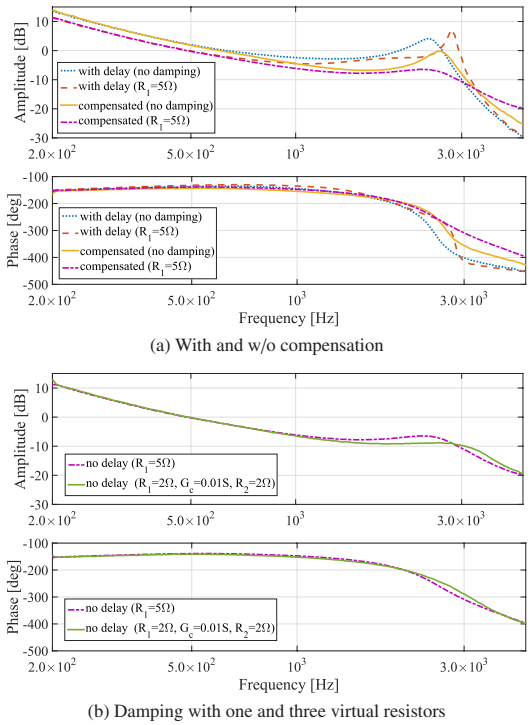

(a) With and w/o compensation

(b) Damping with one and three virtual resistors

Fig. 8. Frequency characteristics of transfer function of the regulated current errors

This validates effectiveness of the proposed delay compensation.

4.2 Active Damping Control with Multiple Virtual Resistors Effects of the proposed damping control with three virtual resistor are also investigated. The measured frequency characteristics of the TFs are shown and compared in Fig. 8(b). Control gains are listed in Table 2(b). The TFs are

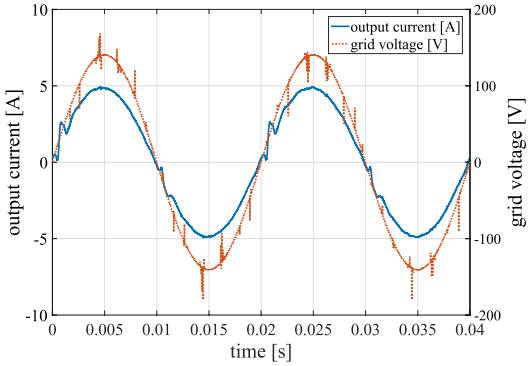

(a) Before the delay compensation and no damping

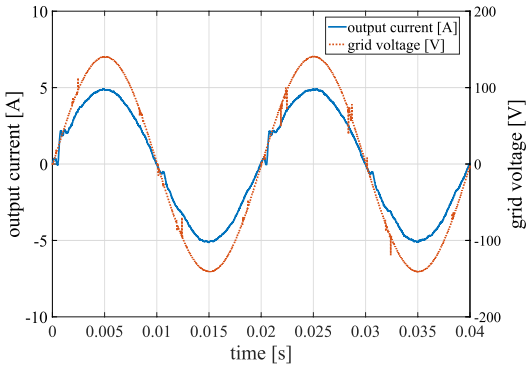

(b) After the delay compensation and no damping

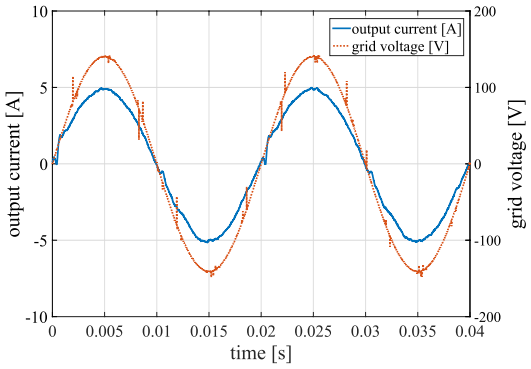

(c) After the delay compensation and one-resistor damping

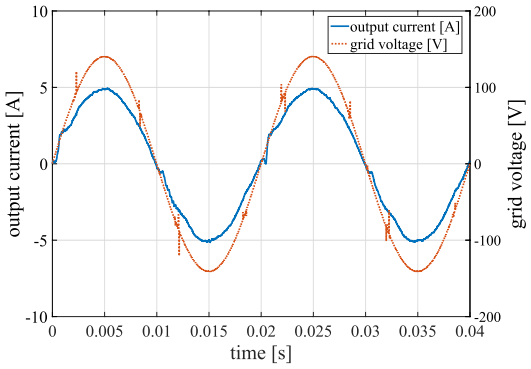

(d) After the delay compensation and three-resistor damping

Fig. 9. Output current and system voltage waveforms

shown as the red dashed curve with the one-resistor damping and as the green curve with the three-resistor damping. The green curve has a smaller peak. The current waveform with the damping with thee-resistor is shown in Fig. 9(d).

The three-resistor damping is more effective than the one-resistor damping. However the differences between them are small. Considering the trade-off between damping effects and control responses and complexity of the methods, the one-resistor damping is practically effective in this case.

5. Conclusions

A control time delay is inevitable for digital control of a grid-connected inverter. The delay should be compensated to make an active damping method effective. This paper proposed a simple and effective delay compensation method and it is applied to the damping control of a grid-connected inverter.

(1) The proposed delay compensation is based on an estimation method of future state values advanced by the delay time.

(2) The proposed compensation method was applied to control of a grid-connected inverter. It is validated that the estimated values coincide with the actual values.

(3) The proposed method was applied to the damping control of a grid-connected inverter. Its effectiveness is investigated and validated for TFs of the regulated current errors by experiment.

(4) The damping method was compared between with one and three virtual resistors. The three-resistor damping is more effective than the one-resistor damping. However the differences between them are small. There is a trade-off between damping effects and control responses. In this case, the one-resistor damping is practically effective.

The proposed compensation method is also applicable to a variety of power electronic system controls and more applications are investigates as future subjects.

Acknowledgment

This work was supported by (MEXT/JSPS) KAKENHI Grant Number JP17K06324.

References

(1) M. Lindgren and J. Svensson: “Control of a voltage-source converter connected to the grid through an LCL-filter-application to active filtering”, IEEE PESC, pp.229–235 (1998)

(2) E. Twining and D.G. Holmes: “Grid current regulation of a three-phase voltage source inverter with an LCL input filter”, IEEE Trans. on Power Electronics, Vol.18, No.3, pp.888–895 (2003)

(3) F. Blaabjerg, R. Teodorescu, M. Liserre, and A. Timbus: “Overview of control and grid synchronization for distributed power generation systems”, IEEE Trans. Ind. Electron., Vol.53, No.5, pp.1398–1409 (2006)

(4) M. Malinowski and S. Bernet: “A simple voltage sensorless active damping scheme for three-phase PWM converters with an LCL filter”, IEEE Trans. on Ind. Electron., Vol.55, No.4, pp.1876–1880 (2008)

(5) J. Dannehl, C. Wessels, and F.W. Fuchs: “Limitations of voltage oriented PI current control of grid-connected PWM rectifiers with LCL filters”, IEEE Trans. Ind. Electron., Vol.56, No.2, pp.380–388 (2009)

(6) J. Dannehl, F.W. Fuchs, S. Hansen, and P.B. Thogersen: “Investigation of active damping approaches for PI-based current control of grid-connected pulse width modulation converters with LCL filters”, IEEE Trans. on Ind. Appl., Vol.46, No.4, pp.1509–1517 (2010)

(7) D. Ricchiuto, M. Liserre, T. Kerekes, R. Teodorescu, and F. Blaabjerg: “Robustness analysis of active damping methods for an inverter connected to the grid with an LCL-filter”, Energy Conversion Congress and Exposition (ECCE), pp.2028–2035 (2011)

(8) X. Wang, F. Blaabjerg, and P.C. Loh: “Analysis and design of grid-current-feedback active damping for LCL resonance in grid-connected voltage source converters”, Energy Conversion Congress and Exposition (ECCE), pp.373–380 (2014)

(9) M. Huang, X. Wang, P.C. Loh, F. Blaabjerg, and W. Wu: “Stability analysis and active damping for llcl-filter-based grid-connected inverters”, IEEJ

Journal of Industry Applications, Vol.4, No.3, pp.187–195 (2015)
(10) Y. Lei, Z. Zhao, H. He, S. Liu, and L. Yin: "An improved virtual resistance damping method for grid-connected inverters with LCL filters", Energy Conversion Congress and Exposition (ECCE), pp.3846–3822 (2011)
(11) S.G. Parker, B.P. McGrath, and D.G. Holmes: "Regions of active damping control for LCL filters", Energy Conversion Congress and Exposition (ECCE), pp.53–60 (2012)
(12) C. Bao, X. Ruan, X. Wang, W. Li, D. Pan, and K. Weng: "Design of injected grid current regulator and capacitor-current-feedback active-damping for LCL-type grid-connected inverter", Energy Conversion Congress and Exposition (ECCE), pp.579–586 (2012)
(13) Y. Tang, P.C. Loh, P. Wang, F.H. Choo, and F. Gao: "Exploring inherent damping characteristics of LCL-filters for three-phase gridconnected voltage source inverters", IEEE Trans. Power Electron., Vol.27, No.3, pp.1433–1443 (2012)
(14) J. He, Y.W. Li, D. Bosnjak, and B. Harris: "Investigation and Active Damping of Multiple Resonances in a Parallel-Inverter-Based Microgrid", IEEE Trans. on Power Electronics, Vol.28, No.1, pp.234–246 (2013)
(15) M.A. Gaafar and M. Shoyama: "Active damping for grid-connected LCL filter based on optimum controller design using injected grid current feedback only", Energy Conversion Congress and Exposition (ECCE), pp.3628–3633 (2014)
(16) T. Kato, K. Inoue, and Y. Akiyama: "Sinusoidal compensator with active damping effects in grid-connected inverter with an LCL filter", Energy Conversion Congress and Exposition (ECCE), pp.4683–4688 (2013)
(17) T. Kato, K. Inoue, Y. Akiyama, and K. Ohashi: "Optimum and adjustable damping control of grid-connected inverter with an LCL filter", International Conference on Power Electronics and ECCE Asia (ICPE-ECCE Asia) pp.123–128 (2015)
(18) R. Li, B. Liu, S. Duan, J. Yin, and X. Jiang: "Analysis of delay effects in single-loop controlled grid-connected inverter with LCL filter", in Proc. IEEE Appl. Power Electron. Conf., pp.329–333 (2013)
(19) X. Zhang, J.W. Spencer, and J.M. Guerrero: "Small-signal modeling of digitally controlled grid-connected inverters with LCL filters", IEEE Trans. Ind. Electron., Vol.60, No.9, pp.3752–3765 (2013)
(20) D. Pan, X. Ruan, C. Bao, W. Li, and X. Wang: "Capacitor-current-feedback active damping with reduced computation delay for improving robustness of LCL-type grid-connected inverter", IEEE Trans. Power Electron., Vol.29, No.7, pp.3414–3427 (2014)
(21) C. Zou, B. Liu, S.Duan, and R. Li: "Influence of delay on system stability and delay optimization of grid-connected inverters with LCL filter", IEEE Trans. Ind. Informat., Vol.10, No.3, pp.1775–1784 (2014)
(22) Y. Lyu, H. Lin, and Y. Cui: "Stability analysis of digitally controlled LCL type grid-connected inverter considering the delay effect", IET Power Electron., Vol.8, No.9, pp.1651–1660 (2015)
(23) D. Yang, X. Ruan, and H. Wu: "A real-time computation method with dual sampling modes to improve the current control performance of the LCL-type grid-connected inverter", IEEE Trans. Ind. Electron., Vol.62, No.7, pp.4563–4572 (2015)
(24) J. Wang, J.D. Yan, L. Jiang, and J. Zou: "Delay-dependent stability of single-loop controlled grid-connected Inverters with LCL filters", IEEE Trans. Power Electron., Vol.31, No.1, pp.743–757 (2016)
(25) H. Deng, R. Oruganti, and D. Srinivasan: "PWM methods to handle time delay in digital control of a UPS inverter", IEEE Trans. Power Electron., Vol.3, No.1, pp.1–6 (2005)
(26) P. Mattavelli, F. Polo, F.D. Lago, and S. Saggini: "Analysis of control delay reduction for the improvement of UPS voltage-loop bandwidth", IEEE Trans. Ind. Electron., Vol.55, No.8, pp.2903–2911 (2008)
(27) Z. Wan, J. Xiong, J. Lei, and C. Chen: "Analyze and reduce the impact of sampling delay on LCL converter with capacitor current feedback active damping", in Proc. IEEE 11th Int. Conf. Power Elect. Drive Syst., pp.539–545 (2015)
(28) C. Chen, J. Xiong, Z. Wan, J. Lei, and K. Zhang: "A time delay compensation method based on area equivalence for active damping of an LCL-type converter", IEEE Trans. on Power Electronics, Vol.32, No.1 (2017)
(29) S. Hyunl, S. Hongl, and C. Wonl: "A compensation method to reduce sampling delay of zero dead-time PWM using 3-Level NPC PWM Inverter", ITEC Asia-Pacific. (2016)
(30) M.G.F. Gous and H.J. Beukes: "Time delay and dead-time compensation for a current controlled four-leg voltage source inverter utilized as a shunt active filter", Conference Record of 39th IAS Annual Meeting, pp.115–122 (2004)
(31) P. Cortes, J. Rodriguez, C. Silva, and A. Flores: "Delay compensation in model predictive current control of a three-phase Inverter", IEEE Trans. Ind. Electron., Vol.59, No.2, pp.1323–1325 (2012)
(32) T. Kato, K. Inoue, and Y. Donomoto: "Fast current-tracking control for grid-connected inverter with an LCL filter by sinusoidal compensation", Energy Conversion Congress and Exposition (ECCE), pp.2543–2548 (2011)
(33) M. Semasa, T. Kato, and K. Inoue: "A time delay compensation method for grid-conncted inverter with an LCL filter", IEEJ Static Power Converter Committee Workshop, SPC-18-033 (2018) (in Japanese)

Appendix

1. Active Damping Control with Multiple Virtual Resistors

The active damping method with one virtual resistor can be extended to a multiple virtual resistor case. The basic idea is very simple that all eigenvalues of the actual and the virtual damping circuits after feedback controls are designed to have identical poles so that their damping effects behave very similarly. For example, the extended damping control can be designed to behave as the circuit with three virtual resistors R_1, R_2, G_C in Fig. 4.

The system equation of the circuit is expressed as follows.

$$\dot{\boldsymbol{x}} = \breve{\boldsymbol{A}}_c \boldsymbol{x} + \boldsymbol{b}_c u + \boldsymbol{h}_c v_s \cdots\cdots\cdots\cdots\cdots\cdots\cdots\cdots\cdots\cdots (A1)$$

where

$$\breve{\boldsymbol{A}}_c = \begin{bmatrix} -\dfrac{R_1}{L_1} & -\dfrac{1}{L_1} & 0 \\ \dfrac{1}{C} & -\dfrac{G_C}{C} & -\dfrac{1}{C} \\ 0 & \dfrac{1}{L_2} & -\dfrac{R_2}{L_2} \end{bmatrix} \cdots\cdots\cdots\cdots\cdots\cdots\cdots (A2)$$

Its system matrix with the state feedback control is as follows where $\breve{\boldsymbol{f}} = [\breve{f}_1 \ \breve{f}_2 \ \breve{f}_3]$.

$$\breve{\boldsymbol{A}}_c - \boldsymbol{b}_c \breve{\boldsymbol{f}} = \begin{bmatrix} -\dfrac{R_1 + \breve{f}_1 E}{L_1} & -\dfrac{1 + \breve{f}_2 E}{L_1} & -\dfrac{\breve{f}_3 E}{L_1} \\ \dfrac{1}{C} & -\dfrac{G_C}{C} & -\dfrac{1}{C} \\ 0 & \dfrac{1}{L_2} & -\dfrac{R_2}{L_2} \end{bmatrix} \cdots\cdots\cdots\cdots\cdots\cdots\cdots (A3)$$

Its characteristic equation becomes as follows.

$$\begin{aligned} |s\boldsymbol{I} - \breve{\boldsymbol{A}}_c + \boldsymbol{b}_c \breve{\boldsymbol{f}}| &= \begin{vmatrix} s - \breve{K}_1 & -\breve{K}_2 & -\breve{K}_3 \\ -\alpha & s - \gamma & \alpha \\ 0 & -\beta & s - \delta \end{vmatrix} \\ &= s^3 - (\gamma + \delta + \breve{K}_1)s^2 \\ &\quad + (\breve{K}_1\gamma + \gamma\delta + \breve{K}_1\delta + \alpha\beta - \breve{K}_2\alpha)s \\ &\quad - \breve{K}_1\gamma\delta - \breve{K}_3\alpha\beta - \breve{K}_1\alpha\beta + \breve{K}_2\alpha\delta \\ &\qquad\qquad \cdots\cdots\cdots\cdots\cdots\cdots\cdots (A4) \end{aligned}$$

where

$$\left.\begin{aligned} &\alpha = \frac{1}{C}, && \beta = \frac{1}{L_2} \\ &\gamma = -\frac{G_C}{C}, && \delta = -\frac{R_2}{L_2} \\ &\breve{K}_1 = -\frac{R_1 + \breve{f}_1 E}{L_1}, && \breve{K}_2 = -\frac{1 + \breve{f}_2 E}{L_1}, \quad \breve{K}_3 = -\frac{\breve{f}_3 E}{L_1} \end{aligned}\right\}$$

The feedback gains $\breve{\boldsymbol{f}} = [\breve{f}_1 \ \breve{f}_2 \ \breve{f}_3]$ can be determined by the optimal control.

The system matrix of the circuit in Fig. 1 is as follows after the state feedback control where $\boldsymbol{f} = [f_1 \ \ f_2 \ \ f_3]$ which is set

to have same eigenvalues of the circuit in Fig. 4.

$$\boldsymbol{A}_c - \boldsymbol{b}_c\boldsymbol{f} = \begin{bmatrix} -\dfrac{f_1E}{L_1} & -\dfrac{1+f_2E}{L_1} & -\dfrac{f_3E}{L_1} \\ \dfrac{1}{C} & 0 & -\dfrac{1}{C} \\ 0 & \dfrac{1}{L_2} & 0 \end{bmatrix} \cdots\cdots\cdots\cdots\cdots\cdots (A5)$$

Its characteristic equation becomes as follows.

$$\begin{aligned} |s\boldsymbol{I} - \boldsymbol{A}_c + \boldsymbol{b}_c\boldsymbol{f}| &= \begin{vmatrix} s-K_1 & -K_2 & -K_3 \\ -\alpha & s & \alpha \\ 0 & -\beta & s \end{vmatrix} \\ &= s^3 - K_1s^2 + (\alpha\beta - K_2\alpha)s \\ &\quad -K_3\alpha\beta - K_1\alpha\beta \cdots\cdots\cdots\cdots (A6) \end{aligned}$$

where

$$K_1 = -\frac{f_1E}{L_1}, \quad K_2 = -\frac{1+f_2E}{L_1}, \quad K_3 = -\frac{f_3E}{L_1}$$

The two sets of the coefficients of (A4) and (A6) are compared so that these constants $K_1 - K_3$ are set to have the same eigenvalues of the resistive circuit.

$$\left.\begin{aligned} K_1 &= \gamma + \delta + \check{K}_3 \\ \alpha\beta - K_2\alpha &= \check{K}_1\gamma + \gamma\delta + \check{K}_1\delta \\ &\quad +\alpha\beta - \check{K}_2\alpha \\ -K_3\alpha\beta - K_1\alpha\beta &= -\check{K}_1\gamma\delta - \check{K}_3\alpha\beta \\ &\quad -\check{K}_1\alpha\beta + \check{K}_2\alpha\delta \end{aligned}\right\} \cdots\cdots\cdots\cdots (A7)$$

$K_1 - K_3$ are calculated from $\check{K}_1 - \check{K}_3$ as follows.

$$\left.\begin{aligned} K_1 &= \gamma + \delta + \check{K}_1 \\ \alpha K_2 &= -\{\check{K}_1\gamma + \gamma\delta + \check{K}_1\delta - \check{K}_2\alpha\} \\ \alpha\beta K_3 &= -\{-\check{K}_1\gamma\delta - \check{K}_3\alpha\beta - \check{K}_1\alpha\beta \\ &\quad +\check{K}_2\alpha\delta + (\gamma + \delta + \check{K}_1)\alpha\beta\} \end{aligned}\right\} \cdots\cdots\cdots\cdots (A8)$$

The state feedback gains with the proposed virtual damping become as follows.

$$\boldsymbol{f} = \left[-\frac{L_1}{E}K_1 \quad -\frac{K_2L_1+1}{E} \quad -\frac{L_1}{E}K_3\right] \cdots\cdots\cdots\cdots (A9)$$

Masaki Semasa (Non-member) was born in Okayama, Japan. He received B.E. and Master's degrees from Doshisha University, Kyoto, Japan, in 2016 and 2018 respectively. Now he works at Chugoku Electric Power Co., Inc. His research interests are control techniques of power electronic systems.

Toshiji Kato (Fellow) was born in Kyoto, Japan. He received his B.E., M.E., and Ph.D. degrees from Doshisha University, Kyoto, Japan, in 1979, 1981, and 1986 respectively. Since 1981, he has been with Doshisha University, where he is now a Professor in the Department of Electrical Engineering. He was a visiting scientist of IREQ from April to August of 1990 and of MIT LEES from 1990 to 1992. His primary interests include computer analysis and control of power and power electronic systems. He is a member of the IEEE, and IEE of Japan.

Kaoru Inoue (Member) was born in Osaka, Japan. He received B.E. and M.E. degrees from Kansai University in 1996 and 1998, respectively. He also received Ph.D. degree from Osaka University in 2001. He was a Research Fellow of the Japan Society for the Promotion of Science from 2000 to 2001. Since 2001, he has been with Department of Electrical Engineering, Doshisha University, where he is now a Professor. He was a visiting scholar of the Department of Electrical Engineering and Computer Science (EECS) at the University of California, Berkeley from 2007 to 2008. His research interest includes analysis and control of power electronic and motor drive systems. He is a member of the IEEE, IEICE, and IEE of Japan.